Distinct modes of cell competition are governed by entropic and energetic properties of mixed cell populations

Daniel Gradeci,[1,2] Anna Bove,[2,3] Alan R. Lowe,[2,4,5,*]
Shiladitya Banerjee,[1,5,*] and Guillaume Charras[2,3,5,*]

[1] *Department of Physics and Astronomy, University College London, London WC1E 6BT, UK*
[2] *London Centre for Nanotechnology, University College London, London WC1H 0AH, UK*
[3] *Department of Cell and Developmental Biology, University College London, London WC1E 6BT, UK*
[4] *Institute for Structural and Molecular Biology, University College London, London WC1E 6BT, UK*
[5] *Institute for the Physics of Living Systems, University College London, London WC1E 6BT, UK*

How cells with different genetic makeups compete in tissues is an outstanding question in developmental biology and cancer research. Studies in recent years have revealed two fundamental mechanisms of cell competition, driven by short-range biochemical signalling or by long-range mechanical stresses within the tissue. In both scenarios, the outcome of cell competition has generally been characterised using population-scale metrics. However, the underlying strategies for competitive interactions at the single-cell level remain elusive. Here, we develop a cell-based computational model for competition assays informed by high-throughput timelapse imaging experiments. By integrating physical cell interactions with cellular automata rules for proliferation and apoptosis, we find that the emergent modes of cell competition are determined by a trade-off between entropic and energetic properties of the mixed tissue. While biochemical competition is strongly sensitive to local tissue organisation, mechanical competition is largely driven by the difference in homeostatic pressures of the two competing cell types. These findings suggest that competitive cell interactions arise when the local tissue free energy is high, and proceed until free energy is minimised.

* Correspondence: shiladitya.banerjee@ucl.ac.uk, a.lowe@ucl.ac.uk, g.charras@ucl.ac.uk

INTRODUCTION

Cell competition is a fitness control mechanism in which less fit cells (the losers) are eliminated from a tissue for optimal survival of the host [1, 2]. First discovered in the *Drosophila* wing disc [3], cell competition has since been observed in many other physiological and pathophysiological conditions, especially in embryogenesis [4] and the development of tumours [5, 6]. While there have been extensive population-scale studies of competition [7, 8], the competitive strategies and their underlying mechanisms at the single-cell level remain poorly understood.

To date, two broad classes of cell competition have been uncovered. Mechanical competition arises when the two competing cell types have different sensitivities to crowding [9]. In this case, the loser cells die cell-autonomously as a result of increasing overall density and loser cells far from the interface with winners may die [8, 10]. By contrast, during biochemical competition, signalling occurs at the interface between two cell types leading to apoptosis of the loser cells [7, 11, 12]. In this case, elimination only occurs in losers that are in direct contact with the winner cells, and the probability of elimination appears to depend on the extent of contact a loser has with winners [13, 14]. As a result, perturbations affecting the strength of intercellular adhesion have been shown to affect the outcome of competition, suggesting that cell mixing is an important factor in biochemical competition [13]. However, rigorously testing these hypotheses remains challenging due to the difficulty of obtaining sufficient time-resolved single cell level information to bridge scales to the whole tissue.

The emergence of automated long-term microscopy and advanced image analysis for segmentation and cell-cycle state recognition now make single cell studies a realistic prospect [10, 15, 16]. These experimental data allow for the characterisation of each cell's environment and enable hypotheses to be formulated regarding the mechanisms of cell elimination. For example, recent work has shown that cell death in a model of mechanical competition is influenced by local cell density as expected, but that, in addition, division of winner cells appears favoured in neighbourhoods with many loser cells [15], something reminiscent of biochemical competition. Therefore, multiple modes of competition may be at play simultaneously and which dominates remains unclear.

One way of testing the dominance of one mechanism over another is through computational or mathematical modelling. While population-scale models of competition based on ordinary or partial differential equations capture the overall behaviour of the tissue [9, 15, 17], they do not provide insights into the influence of local topography, mechanics and cell-cell signalling on the outcome of competition. Cell-resolution computational models [18, 19] are well suited for describ-

ing how the behaviour of single cells and cell-cell interactions lead to population-scale dynamics. However, cell-scale models of competition have not yet been implemented to test different competitive strategies or investigate the physical parameters that are important in competition. This is largely due to the lack of well characterised experimental data as well as technical challenges in implementing basic biological phenomena such as contact inhibition of proliferation [20]. While biochemical and mechanical competition have usually been viewed as separate phenomena acting through completely different mechanisms, they both lead to the elimination of one cell population raising the possibility of the existence of a unified definition of cell competition.

Here we develop a multi-layered, cell-scale computational model to gain a mechanistic understanding of the single-cell mechanisms that govern mechanical competition and decipher the rules of the cellular game. After calibrating the key physical parameters using pure populations of winner and loser cells, we show that competition emerges naturally when the two distinct cell types are mixed and investigate the impact of each interaction and kinetic parameters on the outcome of mechanical cell competition. We then implement a model of biochemical competition based on contact-dependent death that can replicate all current experimental observations and uncover the key parameters influencing biochemical competition. We find that mechanical competition appears controlled by energetic properties of the tissue, whereas biochemical competition is governed purely by the entropy of cell mixing.

RESULTS

Cell-based model for competition.

Our cell-based model for competition consists of two distinct computational layers that simulate: (i) mechanical interactions between cells and the underlying substrate, and (ii) a cellular automaton that makes decisions for cell growth, mitosis and apoptosis (Figure 1A). Physical interactions at the cell-cell and cell-substrate interfaces are simulated using the Cellular Potts Model [21] (Methods). This implementation was preferred to the less computationally costly vertex model [22], because we calibrate our model to our *in vitro* competition experiments [15] that start from a sub-confluent state. In the Potts model, each cell type is assigned a value of adhesion energy with other cells and the substrate, as well as a preferred (target) area, A_T, and a compressibility modulus, λ. While the balance of forces between adhesion and elasticity determines equilibrium cell shapes, changes in cell size during growth, division and apoptosis are controlled by a second computational layer comprising cell automata rules. It is in this layer that cellular decision-making is implemented at

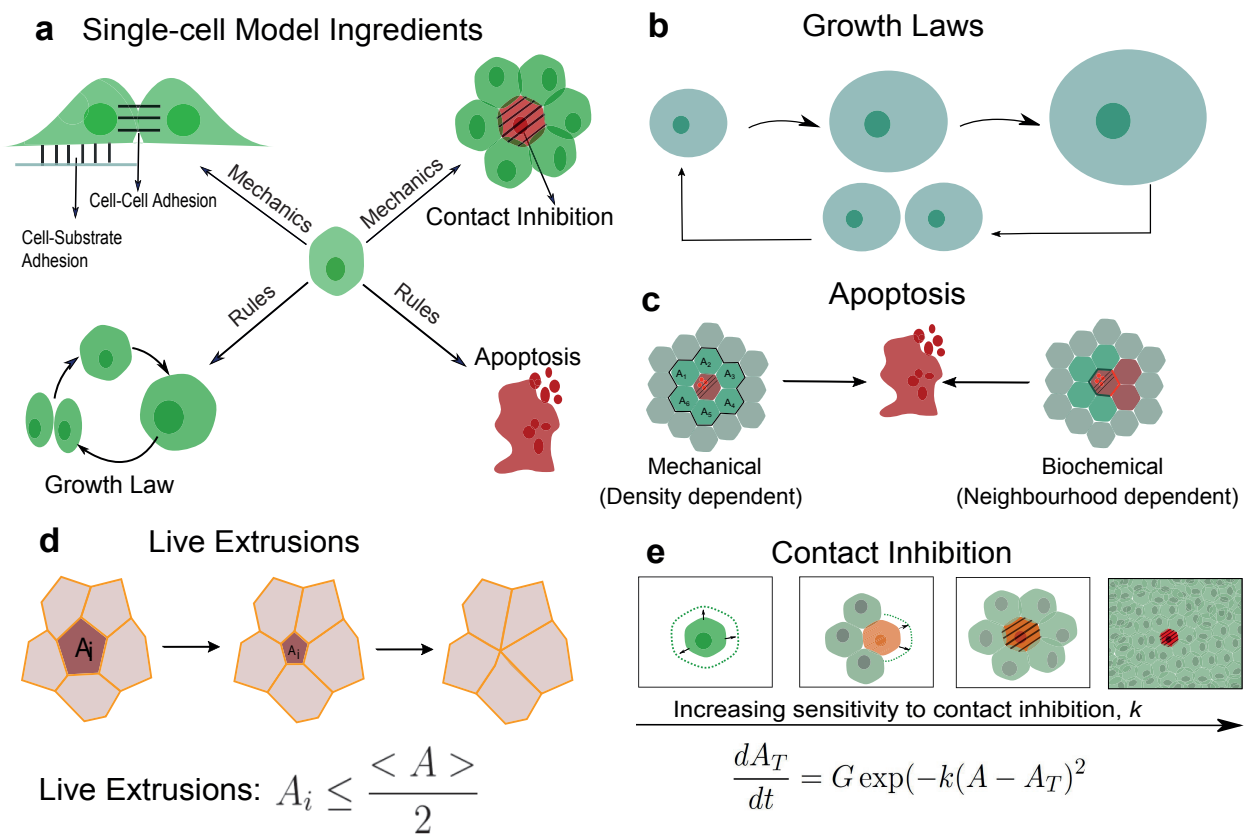

FIG. 1. Physical and decision-making components of the multi-layered computational model. (A) Schematic of the single cell behaviours incorporated into the multi-layered computational model. The first layer modelling the mechanics, such as adhesion and compressibility, is implemented using the Cellular Potts Model. The second layer comprises cellular automata rules describing cell growth, division, apoptosis and contact inhibition. These rules are algorithmically executed for each cell at each time point. (B) Cells grow linearly in time and follow an adder mechanism for division control, in which a threshold size must be added before a cell can divide. (C) Two rules were implemented for apoptosis. One describes the density-dependent cell death observed as in mechanical competition. The other describes the contact-dependent cell death observed in biochemical competition. (D) A rule for live cell extrusion postulates that if a cell's area, A, decreases below half of the mean cell area of the population, $\langle A \rangle/2$, then it is extruded from the monolayer. (E) Schematic depiction of contact inhibition showing cell growth and movement are arrested when local cell density increases.

each time-point based on a set of probabilistic rules (Methods).

To model cell growth during the cell cycle, we increased the cell target area at a constant rate. Cells divide once a threshold area has been added since the start of the cell cycle (Figure 1B), following the adder mechanism of division control recently found for the MDCK cells that we use in our experiments [23]. We implemented two different rules for apoptosis (Figure 1C) for me-

chanical and biochemical competition. Under crowded conditions where mechanical competition is dominant, the probability of apoptosis increases with local cell density (Supplementary Figure 1A), which we determined from our experimental data [15]. In biochemical competition, the probability of apoptosis of loser cells depends on the percentage of their perimeter in contact with the winner cells (heterotypic contact, Supplementary Figure 1B) [13]. Cell elimination could also occur through live cell extrusions [24, 25] when a cell's area, A, dropped below half the average cell area in the simulation (Figure 1D). In addition to the above decision-making rules, we also incorporated contact inhibition of proliferation (Figure 1E), such that the addition of cell area, and consequently division timing, slow down exponentially as the local cell density increases (Methods). To model contact inhibition, we assume that the effective growth rate of the cell depends on the difference between the current cell area and the target area as, $dA_T/dt = Ge^{-k(A-A_T)^2}$, where G is the base growth rate and k quantifies the sensitivity to contact inhibition. Taken together, the combination of cellular mechanics and decision-making strategies provides an integrative computational platform to investigate how the interplay between short-range and long-range competitive interactions determine tissue composition.

Growth and homeostasis of pure cell populations

Having developed a multi-layered computational model for an epithelium, we sought to describe homeostasis in pure cell populations undergoing proliferation and apoptosis. To this end, we calibrated the intercellular adhesion energy $J_{cell-cell}$, the cell-substrate adhesion energy $J_{cell-substrate}$, the area elasticity λ, the growth rate G, and the contact inhibition parameter k for each cell type separately based on our experimental data (Supplementary Table 1). We sought to match the experimentally measured area of cells in sparse conditions to calibrate J and λ, and used the experimentally measured cell doubling time to determine G. The strength of contact inhibition, k (Methods), was chosen such that the cell density at long time scales in simulations reached a plateau that matched the one observed in experiments.

When the simulations were initialised with the calibrated parameters and the same initial cell number as in experiments, cell count and density in the simulations qualitatively reproduced our experimental observations (Figure 2A-B, Supplementary Figure 2, Supplementary movie 1). The MDCK wild type (MDCK^{WT}) cell count increased for 70h before reaching a plateau at a normalised cell count of 5.5, indicative of homeostasis (Figure 2C). The temporal evolution of the average local cell density and the distribution of number of neighbours at confluence were also faithfully replicated by our simulations (Figure 2D-E). An accurate replication of sidedness of cells (Figure 2E) is

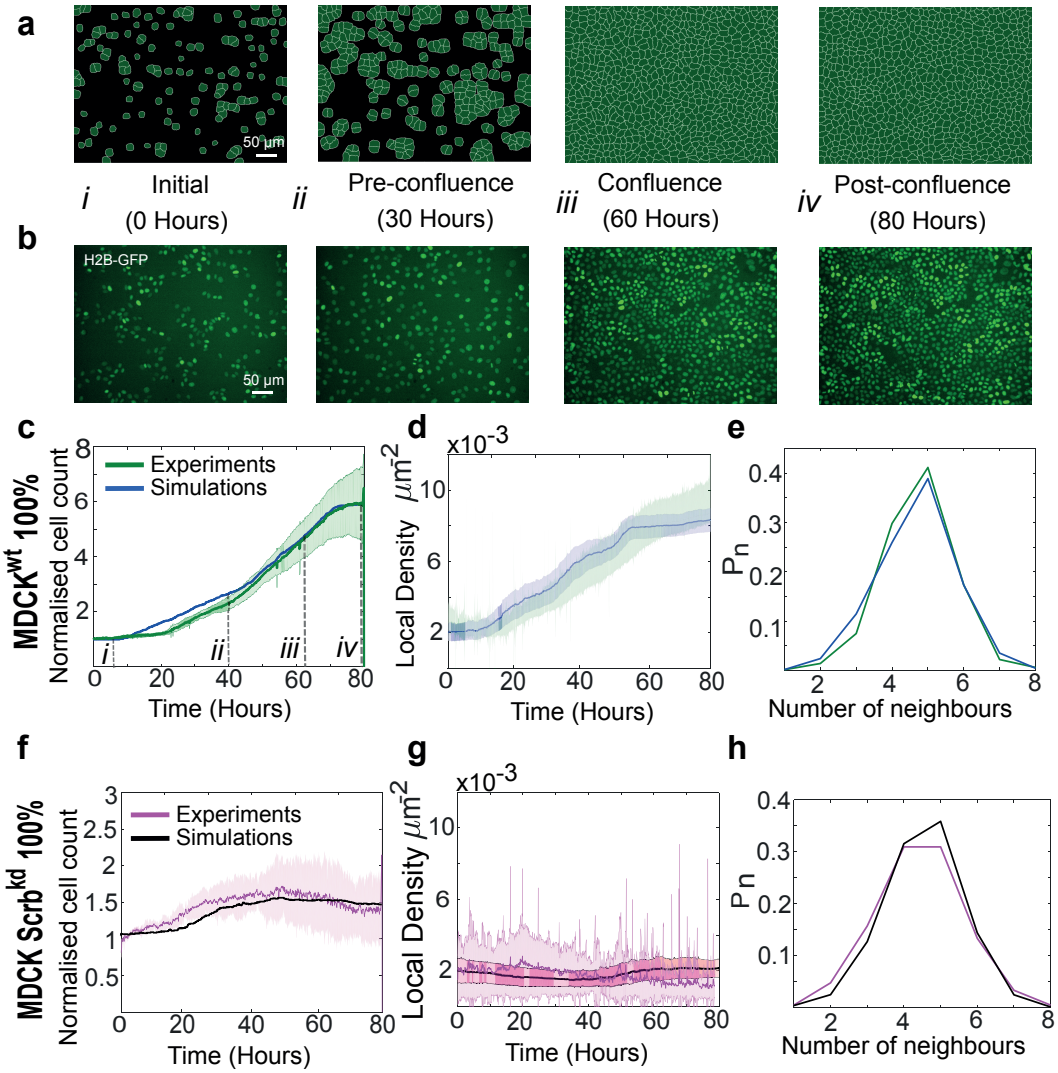

FIG. 2. Model simulations capture the dynamics of growth and homeostasis in pure cell populations. (A) Simulation snapshots of the growth of a pure population of MDCK^{WT} (winner) cells. Each image corresponds to one computational field of view, representing 530 μm $\times$ 400 μm. (B) Experimental snapshots of MDCK^{WT}cells expressing the nuclear marker H2B-GFP. Each image corresponds to 530 μm $\times$ 400 μm and is acquired by wide-field epifluorescence using 20x magnification. The timing of each image is indicated between the two image rows. (C) Normalised cell count as a function of time for winner cells in simulations (blue) and experiments (green). (i-iv) indicate the time points at which the snapshots in (A-B) were taken. (D) Local cellular density as a function of time for the same data as C. (E) Distribution of sidedness of cells post confluence. The curves indicate the proportion of cells as a function of number of neighbours. (C-E) green curves represent experimental data and blue curves simulated data. (F-H) are same as (C-E) for pure populations of loser cells (MDCK Scrib^{kd}). Purple curves are experimental data and black curves represent simulated data. (C-H) Data are pooled from three biological replicates imaging four fields of view each, and from 12 simulations. The solid line indicates the mean and the shaded area indicates the standard deviation.

particularly important for simulating biochemical competition, because the probability of apoptosis of loser cells is linked to the fraction of perimeter occupied by winner cells [13].

Similar to the wild type cells, our parametrisation of loser cells (MDCK scribble^{kd}) accurately replicated the temporal evolution of cell count and density, as well as the distribution of the number of cell neighbours (Figure 2F-H, Supplementary movie 2). In particular, the loser cell count and density stayed fairly constant throughout the experiment, indicative of a lower homeostatic density than the winner cells, as observed in our experiments. This difference in homeostatic density between the winner and the loser cells is necessary for mechanical competition to ensue, as we discuss later.

Model epithelia possess a well-defined homeostatic density

The maintenance of an intact barrier between the internal and the external environment is a key function of epithelia. This necessitates exact balancing of the number of cell deaths and divisions and failure to do so is an early marker of cancer development. Recent work has revealed that epithelia possess a preferred density to which they return following perturbation [24, 26, 27]. In experiments, cells were grown to confluence on stretchable substrates and subjected to a step deformation. When deformation increased cellular apical area, cells resumed division, while a decrease in apical area resulted in live cell extrusion and apoptosis [24]. Therefore, the existence of a homeostatic density is an essential property of epithelia that relates to their sensitivity to crowding, a key factor in mechanical competition.

To test the ability of our model to replicate epithelial homeostatis, we simulated a sudden increase in cell density and its subsequent relaxation, in a confluent epithelium. We replicated experiments in which the cell density of a confluent epithelium grown on a stretched substrate was suddenly increased by 30% via release of the mechanical stretch [24]. In the experiments, the sudden increase in crowding was followed by a gradual decrease in cell density, before returning to the initial homeostatic density after ∼6h (green data points, right panel, Figure 3A, Supplementary movie 3). Decrease in cell number was the result of a combination of live cell extrusions at early times and apoptoses later.

In our simulations, we allowed cells to reach their homeostatic density before suddenly increasing it by an amount similar to experiments. The simulated evolution of cell density faithfully replicated the experimental data, with cell density returning to homeostasis after 6h (blue dots, Figure 2B). In snapshots of the simulations, many live cell extrusions were apparent immediately after the increase in density (red cells, $t = 0$ min, Figure 3A). Thus, our model implementation

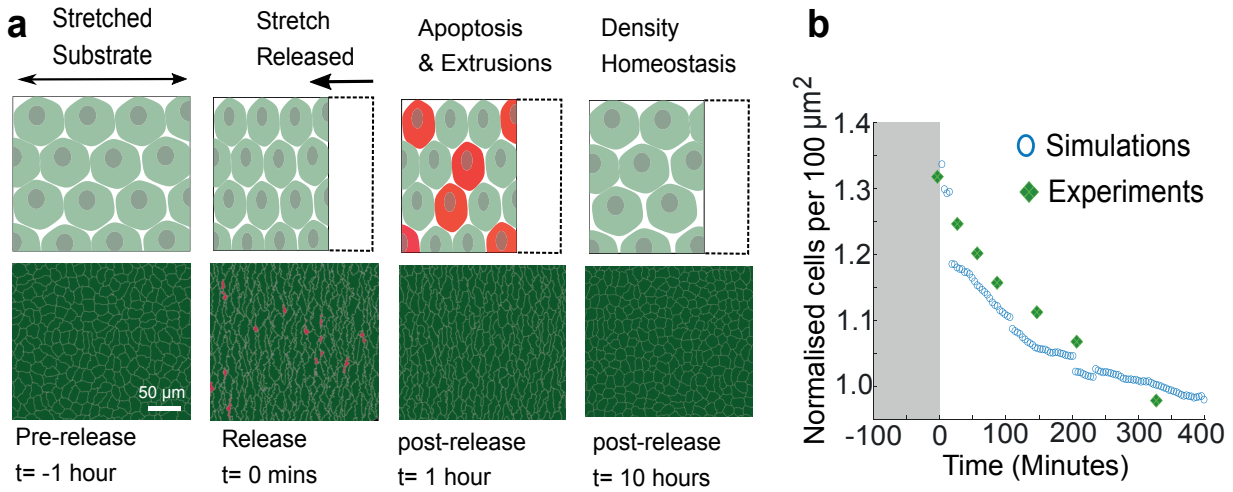

FIG. 3. Return to homeostasis in response to density perturbation. (A) Simulation snapshots of MDCK^{WT} cells grown to confluence on a stretched silicon substrate, and subjected to a sudden increase in density after stretch release. Top row: cartoon diagrams depicting the experiment. Bottom row: snapshots of simulations. Homeostatic density is restored after an increase in cell elimination by either extrusion (red) or apoptosis (blue). (B) Evolution of cell density as a function of time in response to a step increase in cell density at $t = 0$ minutes. Density in simulations is indicated by open blue circles and experimental data are shown by green diamond markers [24].

and parametrisation faithfully replicates all dynamic features of winner and loser cell populations, including their ability to reach a homeostatic density after mechanical perturbation.

Mechanical competition is an emergent property of mixed cell populations with different homeostatic densities

Having accurately parametrised our cell-based model to reproduce the dynamics of pure cell populations, we asked if winner and loser cells would compete when placed in mixed populations. We initialised our simulations by seeding a 90:10 winner-to-loser cell ratio. Strikingly, our simulations were able to quantitatively reproduce the experimental data for competition dynamics, with no further adjustment in parameters.

As in the experiments, simulated winner cells (green) rapidly proliferated while loser cell numbers (red) remained roughly constant before diminishing (Figure 4A-B, Supplementary movie 4). Furthermore, the evolution of cell count was quantitatively replicated over the entire duration of the experiment for both winner and loser cells (Figure 4C). When loser cells underwent apoptosis, this was accompanied by the formation of a rosette structure around the dying cell that mirrors what is observed in experiments that visualise cell boundaries [28, 29] (Figure 4E-F). One of the

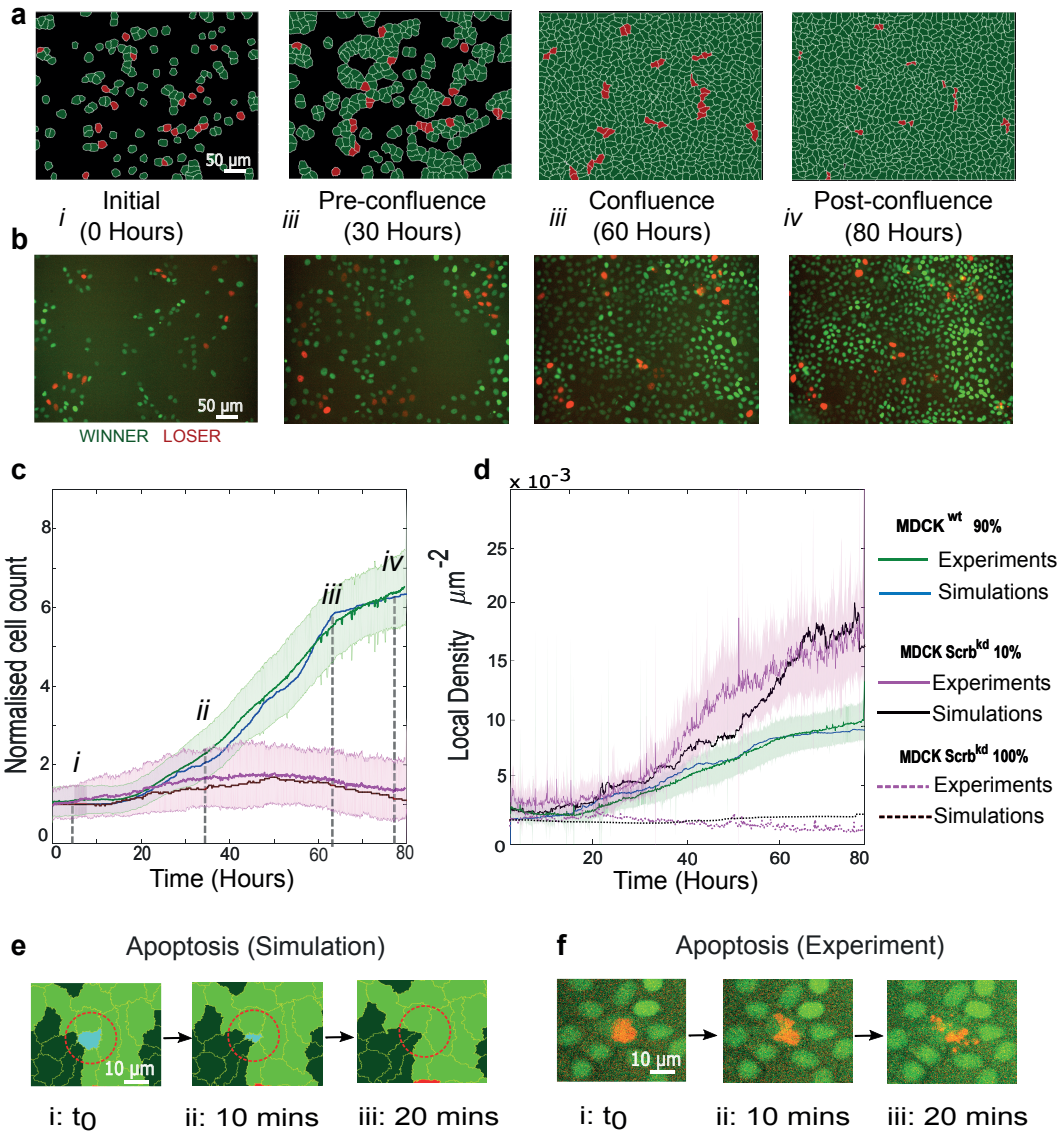

FIG. 4. Cell competition is an emergent property in co-cultures of cells with different homeostatic densities. (A) Simulation snapshots of competition between 90% winner (green) and 10% loser cells (red). Each image corresponds to 530 μm $\times$ 400 μm. (B) Experimental snapshots of competition between 90 % winner cells (green) and 10% loser cells (red) over time. Winner cells (MDCK^{WT}) express the nuclear marker H2B-GFP, while loser cells (MDCK Scrib^{kd}) express the nuclear marker H2B-RFP. Each image corresponds to 530 μm $\times$ 400 μm, and is acquired by wide-field epifluorescence using 20x magnification. The timing of snapshots is indicated in between the two rows of images. (C) Evolution of normalised cell count for winner cells (simulations: blue line, experiments: green line) and loser cells (simulations: black line, experiments: purple line) in experiments initiated with a 90:10 ratio of winner:loser cells. Data are pooled from three biological replicates imaging four fields of view for the experiments and from 12 simulations. Solid lines indicate the means and the shaded areas indicate the standard deviations from experiments. (i-iv) indicate the time points at which the snapshots in (A-B) were taken. (D) Temporal evolution of the local cell density. (E-F) Snapshots of simulations (E) and experiments (F) showing apoptosis of a loser cell (E: blue, F: red) surrounded by winner cells (green).

most striking features of experimental data is that the local density of loser cells increases dramatically compared to pure populations (∼5 fold increase, magenta curve, Figure 4D), while the local density of winner cells follows the same trend as in pure populations (green curve, Figure 4D) [15]. The increase in local density of loser cells is replicated in our simulations and is due to their lower stiffness modulus, λ. In the experiments, the increased local density of loser cells is accompanied by an increase in their height [8], suggesting preservation of cell volume and that λ should be interpreted as an out-of-plane deformability modulus. Thus, differences in homeostatic densities alone appear sufficient to replicate the evolution of cell count and density observed in competition between MDCK^{WT} and MDCK scribble^{kd} [15], suggesting that mechanical competition is the dominant mechanism in these experiments.

Differences in homeostatic density and relative cell stiffness control the outcome of mechanical cell competition

Our simulations indicate that mechanical competition between the two cell types results from the combination of two factors: the lower stiffness λ of the loser cells that leads to their compaction, and their increased sensitivity to crowding (Supplementary Figure 3), both parameters directly calibrated from experimental data. To test this further, we investigated how changes in the contact inhibition parameter k and cell stiffness λ altered the outcome of mechanical competition. In our simulations, sensitivity to contact inhibition was chosen to be the same for both cell types and it constrains how far cells can deviate from their target area before they quiesce (Methods). In pure winner cell populations, homeostatic density decreased with increasing contact inhibition (Figure 5A). However, this effect was not present in pure loser populations (Figure 5A) because their probability of apoptosis is high even for densities below the homeostatic density dictated by k (Supplementary Figure 1A). Indeed, under normal growth conditions, loser cells never reach densities where contact inhibition becomes active. In all cases, the homeostatic density of winner cells was higher than in loser cells but the difference (ΔHD) decreased with increasing k (Figure 5A). Thus, in winner cells, homeostatic density is controlled by the contact inhibition parameter k, while in loser cells it is controlled by their sensitivity to crowding (Supplementary Figure 1A).

When we varied the homeostatic density of the winner cells (by changing k), we found that loser cells were completely eliminated for high values of winner cell homeostatic density but they survived when winner homeostatic density was lower (Figure 5B-C, E). In addition, the time required for elimination of 50% of loser cells increased with decreasing difference in homeostatic density (Figure 5A, F). Therefore, the difference in homeostatic density, ΔHD, between the winner

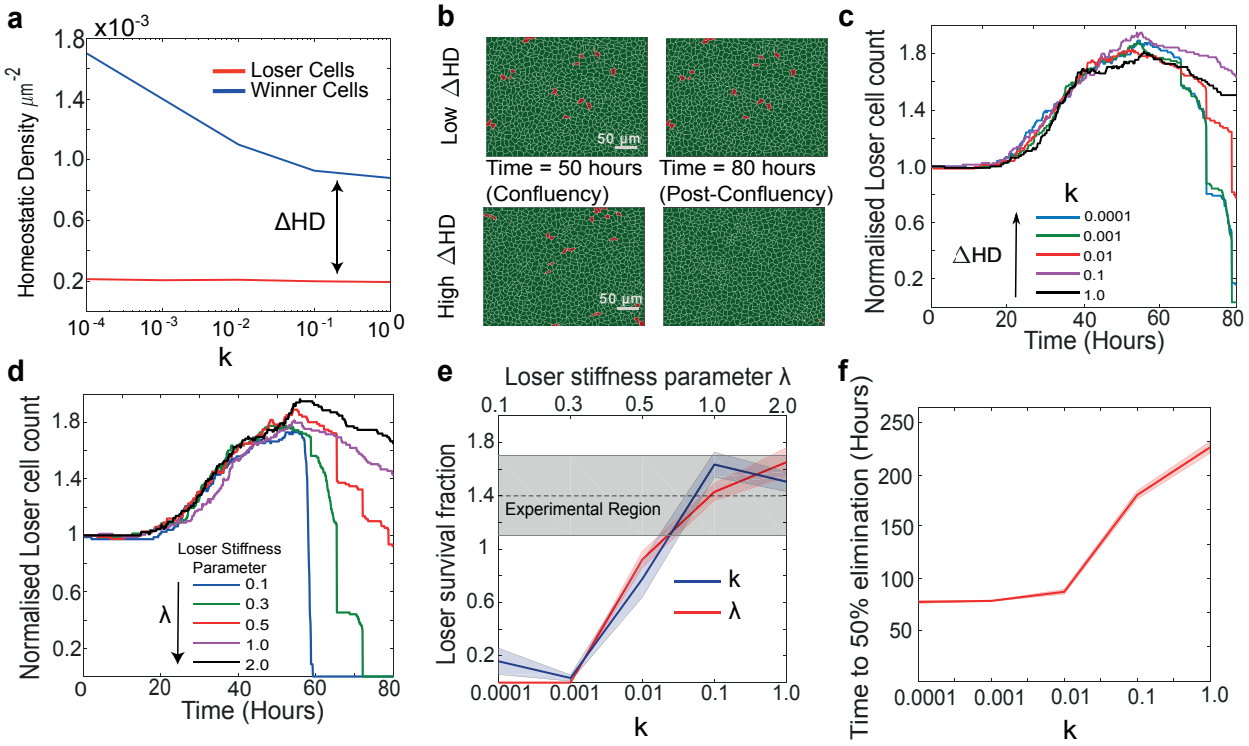

FIG. 5. Cellular stiffness and sensitivity to contact inhibition control the outcome of mechanical competition. (A) Evolution of homeostatic density as a function of the parameter k, quantifying the sensitivity to contact inhibition. Data are shown for pure populations of winner (blue) and loser (red) cells. (B) Simulation snapshots of competition between 90 % winner cells (green) and 10% loser cells (red). The top two panels show the population evolution for a small difference in homeostatic density ΔHD between the two cell types. The bottom two panels show the population evolution for a large ΔHD between the two cell types. Each image corresponds to 530 μm $\times$ 400 μm. (C) Normalised cell count for loser cells in competition simulations for different values of the contact inhibition parameter k. (D) Normalised cell count for loser cells in competition simulations for different values of their stiffness parameter λ. Winner cells have a fixed stiffness of 1.0. Snapshots of competition are shown in Supplementary figure 3A-B. (E) Loser cell survival fraction after 80 hours in simulations run with different parameters for stiffness (red line) and contact inhibition (blue line). Shaded blue and red regions denote the standard deviation. The gray shaded region indicates the survival fraction of loser cells observed in experiments after 80h. (F) Time to 50% elimination of loser cells as a function of the contact inhibition parameter. The solid line indicates the mean and the shaded regions the standard deviation.

and loser cells governs the kinetics and the outcome of mechanical competition (Figure 5A, C, F).

As the winner cells have a higher stiffness λ, they likely impose their homeostatic density on the whole population, leading to increased apoptosis of loser cells. To test this hypothesis, we varied the loser cell stiffness while maintaining winner cell stiffness constant. When loser cell stiffness was lower than the winner cell stiffness, loser cells were eliminated (Supplementary Figure 5A). By

contrast, when the loser cell stiffness was equal to or larger than the winner cell stiffness, loser cells survived (Supplementary Figure 4A, Figure 5D). Akin to ΔHD, changes in the ratio of winner-to-loser cell stiffness altered the kinetics of competition (Figure 5D). In both cases (when ΔHD was high or loser cell stiffness was high), the change in outcome occurred because of a decrease in the density of loser cells under competitive conditions, which in turn led to decreased apoptosis. Furthermore, winners have an extra competitive edge because when free space becomes available due to cell death or cell area compressibility, they are more susceptible to take advantage of the free space due to faster growth, using a *squeeze and take* or a *kill and take* tactic [16].

Other simulations parameters had little impact on mechanical cell competition. We found that the growth rate of loser cells controlled the time to elimination and the peak loser cell count but did not affect the outcome of competition (Supplementary Figure 3D-E). Overall, our simulations suggest that mechanical competition is entirely dependent upon parameters affecting the stored mechanical energy, λ and k.

Entropy of cell mixing governs the outcome of biochemical competition

Our cell-based model can also be used to gain mechanistic insights into biochemical competition. Recent work has shown that, during biochemical competition, apoptosis in loser cells is governed by the extent of their contact with the neighbouring winner cells [13]. Furthermore, perturbations that increased mixing between cell types increased competition [13].

To study biochemical competition in isolation from any mechanical effect, we assumed that both cell types have identical stiffnesses, sensitivity to contact inhibition, and a high homeostatic density. In both cell types, we modelled the dependency of apoptosis on the proportion of cell perimeter engaged in heterotypic contact by using a Hill function parametrised by a steepness S and an amplitude A (Supplementary Figure 1B). When S decreases, the probability of apoptosis increases rapidly with the extent of heterotypic contact (Supplementary Figure 4C). For winner cells, we chose a low A and high S because we do not expect their apoptosis to show sensitivity to contact with loser cells. In contrast, for loser cells, we chose A to be ten-fold higher, giving an amplitude similar to the maximal probability of apoptosis observed in losers during mechanical competition (Supplementary Figure 4C, Supplementary Figure 1A). First, we assumed a homogenous seeding of each cell type with a 50:50 ratio between winners and losers and examined the dependency of outcome on S in loser cells. Loser cells first increased in number until overall confluence, before decreasing after that. When S was low, losers were eliminated (Supplementary Figure 4A, D), whereas when S was high, the two cell populations coexisted and no competition took place

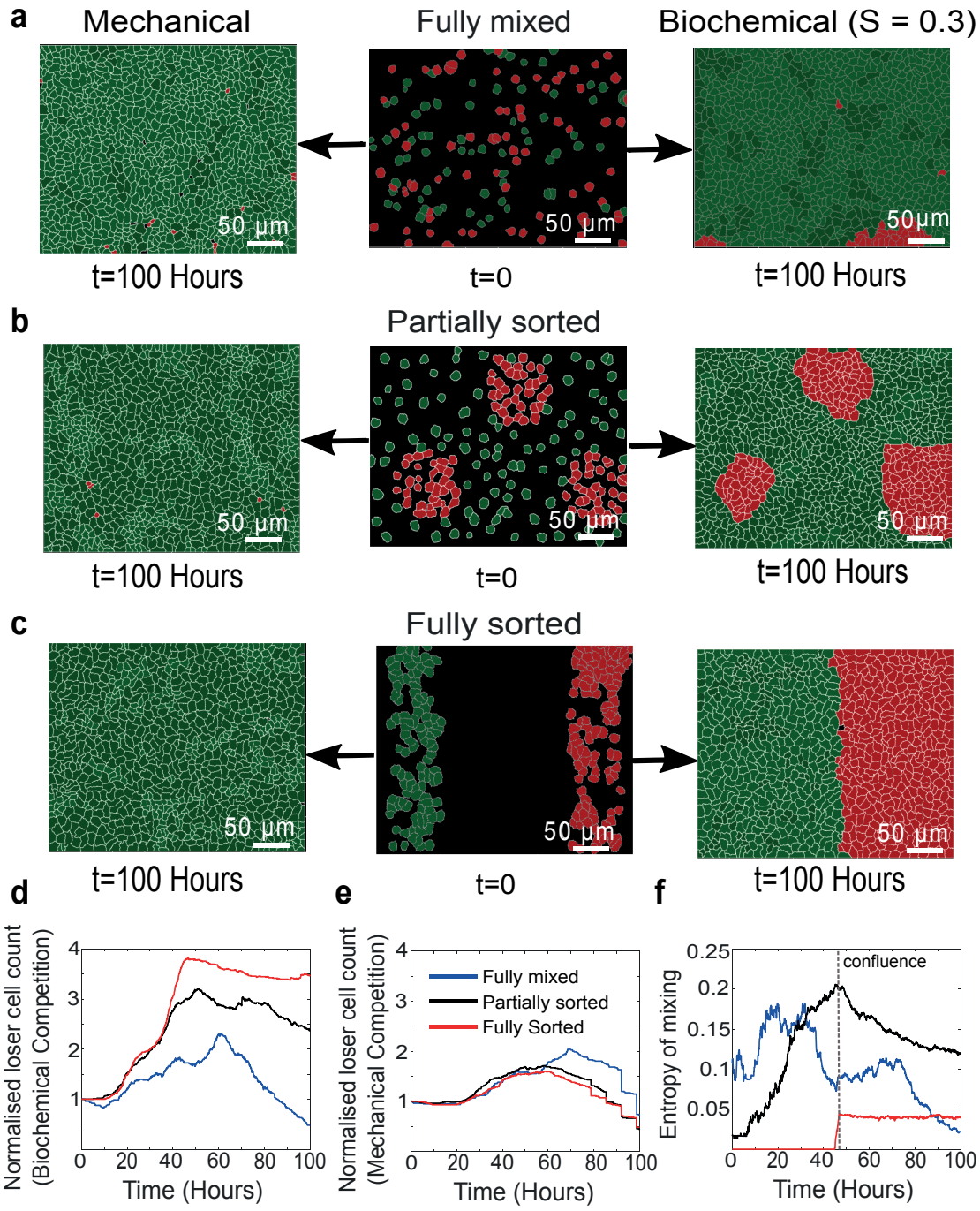

FIG. 6. Tissue organisation and intercellular adhesions govern the outcome of biochemical competition. (A-C) The middle panels show the initial configuration of a competition between 50% loser (green) and 50% winner (red) cells for various seeding arrangements (fully mixed, partially sorted, fully sorted). The right panels show the outcome of competition for biochemical competition. The left panels show the outcome of competition for mechanical competition. Cells are initially separated by free space (black). (D) Normalised proliferation profiles of loser cells from the three configurations for biochemical competition (5A-C, right hand column). (E) Normalised proliferation profiles of loser cells from the three configurations for mechanical competition (5A-C, left hand column). (F) Temporal evolution of the entropy of cell mixing for the three different configurations).

(Supplementary Figure 4B).

Next, we investigated dependency of cell competition on initial seeding conditions for the same simulation parameters. We examined three different conditions: fully mixed (Figure 6A, middle column, Supplementary movies 5-6), partially sorted (with loser cells grouped into a few colonies, Figure 6B, middle column, Supplementary movies 7-8), and fully sorted (with loser cells and winner cells occuping opposite sides of the field of view, Figure 6C, middle column, Supplementary movie 9). Strikingly, while loser cells were always eliminated for mechanical competition (Figure 6A-C, left hand column, Figure 6E), the outcome of competition was strongly dependent on seeding in biochemical competition (Figure 6A-C, right hand column, Figure 6D). Indeed, whereas loser cells were eliminated for fully mixed seeding, they coexisted with winner cells for partially and fully sorted seedings. This suggests that biochemical competition is sensitive to mixing entropy of cells. When we computed the evolution of mixing entropy in each competition (Methods), we found that, when cells reached confluence, entropy was highest in the fully mixed seeding and lowest in the fully sorted seeding (Figure 6F). In all cases, entropy decreased after overall confluence as the competition progressed (Figure 6F). Colony size and geometry therefore determine the impact of biochemical competition. Small colonies of loser cells have a high curvature and each loser cell at the colony interface comes into contact with several winner cells, leading to increased competition. In contrast, in the fully sorted conditions, the interface between loser and winner cells has a low curvature such that loser cells do not contact a sufficient number of winner cells to be eliminated.

In contrast to mechanical competition where energetic parameters governed the outcome of competition, we found that the outcome of biochemical competition was controlled by mechanisms that affected the intermixing of cells. When we examined how changes in heterotypic adhesion (adhesion energy between winner and loser cells), $J_{\text{heterotypic}}$, affected the outcome of competition, we found that the final loser cell count decreased with decreasing $J_{\text{heterotypic}}$ (Supplementary Figure 5B,D,F). This is because for low $J_{\text{heterotypic}}$, cell intermixing is favoured and winner cells can invade colonies of loser cells(Supplementary Figure 5A-D), consistent with experimental observations [13]. However in the fully sorted configuration, where the entropy of mixing is initially zero and remains small after confluence because of the minimisation of interface between the two cell types (Figure 6F), changes in $J_{\text{heterotypic}}$ only have a weak effect (Supplementary Figure 5E-F). Thus, biochemical competition appeared primarily governed by entropic factors. In summary, our simple implementation of biochemical competition was sufficient to qualitatively reproduce experimental observations, although the precise experimental curves relating probability of apoptosis to extent of heterotypic contact remain to be accurately determined experimentally.

DISCUSSION

In this study, we developed a cell-based computational model for competition that allows investigation of the interplay between physical cell interactions and probabilistic decision-making rules on controlling the outcome cell competition. Using this model, we identify the physical and geometrical parameters that influence the outcome of mechanical and biochemical cell competition. Our analysis reveals that the outcome of biochemical or comparative fitness competition is governed by the entropy of mixing between the cell types, whereas the outcome of mechanical competition is controlled by the difference in homeostatic density of the two cell types together with energetic parameters.

Calibration of our model parameters separately for pure populations of winner and loser cells allowed us to quantitatively reproduce the experimentally measured kinetics of cell proliferation, mechanics of tissue homeostasis, as well as the topology of tissue organisation. Strikingly, mechanical competition emerged in mixed populations of MDCK^{WT}(winner) and MDCK scrib^{kd} (loser) cells with no further adjustments to the model parameters. Winners and losers differed in their compressibility modulus λ, their growth rates G, and their probability of apoptosis as a function of density. The latter is directly measured in our experiments [15] and is consistent with the increased sensitivity to crowding in loser cells due to interplay between stress pathways [8, 30]. Our simulations further showed that the growth rate of individual cells controls the kinetics of competition but not its outcome. Varying the growth rate of loser cells led to an increase in the maximal loser cell count, and in elimination time but this did not affect the final outcome of mechanical competition (Supplementary Figure 3E). Overall, only two factors governed the outcome of mechanical competition: the compressibility parameter λ, and the sensitivity to contact inhibition quantified by the parameter k.

The contact inhibition parameter k regulates the rate of cell growth and proliferation post-confluence (Methods). In winner cells, this effect translates into the control of homeostatic density, which is lower for high sensitivity to contact inhibition. However, k does not control homeostatic density in loser cells, due to their increased probability of apoptosis under crowding conditions. As a result, when k is increased, the difference in homeostatic density between the winners and losers, ΔHD, decreases. This leads to slowing of the kinetics of mechanical competition, eventually ceasing altogether. Thus, our simulations predict that ΔHD, which is related to the difference in homeostatic pressure [31], is a good predictor for the outcome of mechanical competition.

Our model parametrisation leads to loser cells that are typically more compressible (or softer)

than winners. As a consequence, in competition assays, loser cells tend to decrease their apical areas after confluence. This higher local density, together with losers' higher sensitivity to crowding, results in preferential elimination of loser cells. Conversely, when losers are stiffer than winners, their local density does not increase dramatically and they survive. Thus, a relative stiffness parameter, $\Lambda = \lambda_{\text{loser}}/\lambda_{\text{winner}}$, emerges as a key control parameter for mechanical competition. Loser cells tend to be eliminated if $\Lambda < 1$, whereas they survive for $\Lambda > 1$. Although by convention λ is referred to as an area compressibility modulus, cells are three-dimensional objects and their volume is tightly regulated even when subjected to mechanical deformations [32, 33]. Thus, the decrease in apical area of loser cells in competition implies a concomitant increase in cell height, consistent with experimental observations [8]. Therefore, λ should be understood as a height elasticity that may emerge from the ratio of apical to lateral contractility that governs the height of epithelial cells in 3D vertex models [34, 35]. Overall, both contact inhibition of proliferation and planar cell compressibility altered the outcome of mechanical competition by changing the local density attained by the loser cells. Thus, mechanical competition appears to be primarily regulated by parameters controlling the compressional mechanical energy stored in the system. Finally, our simulations suggest that the interaction between MDCK^{WT} and MDCK scrib^{kd} cells in our experiments [15] can be entirely explained by mechanical competition alone despite suggestions that biochemical competition may play a role.

Biochemical competition, on the other hand, depends on the proportion of heterotypic contact between losers and winners. As a result, the outcome of biochemical condition strongly depends on the topological organisation of the epithelium but is not affected by changes in cell compressibility or contact inhibition. Instead, two entropic parameters controlled the outcome of biochemical competition: the heterotypic adhesion energy and the initial organisation of the tissue. Indeed, tissue organisations with greater mixing between the cell types resulted in greater elimination of the loser cells (Figure 6). This arises as a natural consequence of the probability of apoptosis of loser cells depending on the extent of heterotypic contact. As a result, tissue organisations where cells were highly mixed led to more competition than those were the two populations are more sorted. In other words, competition depends on the entropy of cell intermixing. Consistent with this, increasing the heterotypic adhesion energy led to more mixing between cell types and more cell competition. Interestingly, experimental evidence has revealed that perturbations that promote cohesion of losers protect against elimination, while those that promote intercalation of winners and losers promote greater elimination [13]. In purely biochemical competition, our simulations reveal the existence of a critical colony radius necessary for survival that depends strongly on the

shape of the function relating the probability of apoptosis to fraction of perimeter in heterotypic contact (Supplementary Figures 4-5). Overall, biochemical competition was favoured in systems with high entropy of mixing but downregulated in systems with lower entropy. While cells did not possess high motility in our simulations, we would expect this to affect the outcome of biochemical competition, as motility would increase entropy of mixing. Overall, our simple implementation of biochemical competition is sufficient to qualitatively replicate current experimental data.

In summary, our study revealed that mechanical competition is governed by factors that reduce the stored mechanical energy in the system, while biochemical competition is favoured by factors that increase the entropy of cell mixing. Mechanical competition did not appear to be affected by entropic factors, whereas biochemical competition was not sensitive to parameters that changed the stored mechanical energy of the tissue. Together, these data suggest a unified definition for cell competition as a process that takes place when the free energy of the system is high and seeks to reduce this. Such a thermodynamic interpretation would further predict that conditions in which we observe coexistence of cell populations are metastable, which has implications for the design of treatment plans in the form of pulses of drug. Future work will be necessary to test these hypotheses in experimental systems.

METHODS

Cellular Potts model. The cellular Potts model is implemented in compucell3D [36]. We chose a 2D lattice-based model, where cells are composed of a collection of lattice sites (pixels). Cells interact at their interfaces through pre-defined adhesion energies and several different cell types can be implemented. Each cell is then given attributes that are crucial for their mechanical properties. For example, each cell is assigned a cell type τ, which in turn has some value of adhesion energy J with other cell types and the substrate. Cells are also assigned a target area A and an area expansion modulus λ, which are important in the implementation of growth and division dynamics. In addition, we also incorporate active cell motility. The free energy of the system is given by the Hamiltonian H:

$$\begin{aligned} H = &\sum_{<i,j>} J[\tau(\sigma^k_{i,j}), \tau(\sigma_{i',j'})](1 - \delta_m(\sigma^k_{i,j}, \sigma_{i',j'})) \\ &+ \lambda \sum_{\sigma} (A(\sigma^k) - A_T(\sigma^k))^2 \Theta(\tau) \\ &+ \lambda_m \sum_{\sigma} \hat{m}(\sigma, t) \cdot \hat{s} \ , \end{aligned} \tag{1}$$

where the first term describes the interaction of lattice sites due to the adhesion energy between the cell types. The coefficient J is the adhesion energy between cell type τ of the target lattice site $\sigma^k_{i,j}$ and the cell type $\tau(\sigma_{i',j'})$ of its nearest neighbour lattice points. The multiplicative term $(1 - \delta_m(\sigma^k_{i,j}, \sigma_{i',j'}))$ prevents cells from interacting energetically with themselves, where:

$$\delta_{ij} = \begin{cases} 1, & \text{if } \sigma^k_{i,j} = \sigma_{i',j'}, \\ 0, & \text{if } \sigma^k_{i,j} \neq \sigma_{i',j'}. \end{cases} \tag{2}$$

The second term in the Hamiltonian describes an additional energy cost due to deviation of the actual area $A(\sigma)$ of a cell from its target area $A_T(\sigma)$, specific to the cell type. The coefficient λ represents the area expansion modulus in 2D, which is related to planar cell stiffness or the ratio between apical and lateral contractility that control cell height. We introduce the term $\Theta(\tau)$ to treat the free space pixels differently from the cell pixels. In contrast to cells, the free space does not have a target area, and hence no associated mechanical energy.

$$\Theta_\tau = \begin{cases} 1, & \text{if } \tau(\sigma^k_{i,j}) = 0 \text{ (free space)}, \\ 0, & \text{Otherwise .} \end{cases} \tag{3}$$

The final term in the Hamiltonian assigns active motility to the cells along a random unit vector $\hat{m}$ [37]. Here $\hat{s}$ is the spin flip direction between the lattice site in question and one of its neighbouring lattice sites.

Model parametrisation. To describe epithelial cell dynamics using the Potts model, we parametrised it using our experimental data [15]. For simplicity, we chose the same length scale for pixels in our simulation as in our experimental images of competition experiments. The lattice size and cell sizes are chosen to match the experimental data. The lattice is chosen to be 1200x1600 pixels, where each pixel is 0.33 μm. The target area of each cell type was determined based on the average cell areas measured from the images of each cell type plated in sparse conditions such that the cells are isolated from one another. A conversion between experimental time and computational time was derived empirically by comparing the mean squared displacements of cells in experiments with that in the simulations. We found that 10 Monte Carlo time steps (MCS) represented 1 frame of a timelapse movie in our experiments (4 mins).

Cell growth and division. The next layer of the model requires the introduction of cellular behaviour in the form of probabilistic rules for cell growth, division, extrusion, and apoptosis. In

our simulations, cells grow linearly by increasing their target areas at a constant rate. Cell growth rate was chosen to replicate the average cell doubling time measured in experiments [15]. In line with recent experimental work [23], we assume that MDCK cells follow an "adder" mechanism for cell size control, such that cells divide along their major axis once a threshold volume has been added. In our simulations, the added cell volume was normally distributed around the mean experimental value, so as to capture cell-to-cell variability. When the simulation was initialised, cell areas had a homogenous distribution ranging from 0.5 to 1 times the threshold volume for division to mimic the distribution of cell ages at the start of experiments.

Contact inhibition of proliferation. Above a certain cell density, proliferation all but ceases, a phenomenon known as contact inhibition of proliferation [20, 38]. An implication of this process is the existence of a homeostatic density for each cell type. Arrest in proliferation is accompanied by a decrease in protein synthesis due to a drop in ribosome assembly and downregulation of the synthesis of cyclins [39]. In our simulations, cells possess a target area, A_T, which they would occupy if they had no neighbours, and an actual current area, A. As the target area of cells increases at each time step, the difference between their target and current area increases. If this difference becomes too large, the second term of the Hamiltonian dominates leading to energetically unfavourable swaps and a collapse of the network. To mimic reduced protein synthesis during contact inhibition of proliferation, we assume that the effective growth rate depends on the difference between the current cell area and the target area:

$$\frac{dA_T}{dt} = G \exp(-k(A - A_T)^2) \ , \tag{4}$$

where G is the base growth rate, A_T the target cell area, A the current area, and k quantifies the sensitivity to contact inhibition, which parametrises how much deviation can be tolerated between the target area and current cell area. Note that this condition is applied iteratively at every frame for each cell, such that when free space becomes available growth can resume nearby.

Apoptosis due to competition. In crowded conditions such as those present in mechanical competition, the probability of apoptosis increases with local cell density [8, 15, 24]. To implement this, each cell was assigned a probability of apoptosis at each time step. The probability of apoptosis depended on the local cell density, which we determined using experimental data for each cell type [15] (Supplementary Figure 1A-B). In biochemical competition, apoptosis occurs when loser cells are in direct contact with winner cells. Recent work has shown that in Drosophila,

the probability of apoptosis of loser cells depends on the percentage of the perimeter in contact with the winner cells [13]. Following this, we chose to implement the probability of apoptosis as a sigmoid function (Hill function) following the relationship $P_{apo}(p) = V_{max}p^n/(S^n + p^n)$, where p is the percentage of perimeter in heterotypic contact, n is the hill coefficient, V_{max} is the maximum probability, and S is the half maximum probability. We chose a maximum probability V_{max} of death per frame similar to that encountered in mechanical competition. (Supplementary Figure 1C). This is justified by the fact that mechanical and biochemical competition take comparable amounts of time in MDCK cells [40, 41]. For both mechanical and biochemical competition, apoptosis was implemented by setting the target area of the cell to zero and area expansion modulus to 2.0. This allows for a quick but not instantaneous decrease of the cell area until the cell is completely removed.

Live extrusion of cells. Under conditions where the local cell density increases rapidly, live cells can be extruded from monolayers, likely because they have insufficient adhesion with the substrate to remain in the tissue [24, 25] (Figure 1D). We assumed that cells underwent live extrusion when their area dropped below half of the average cell area at that time point: $A_i \leq \langle A \rangle/2$. Once a cell is committed to extruding, it is eliminated immediately from the tissue. Unlike apoptosis elimination from extrusion is an instantaneous deletion of the qualifying cell from the lattice.

Comparison to experimental data. All simulated data for mechanical competition were compared quantitatively to experiments acquired in [15]. Methods for data acquisition, segmentation, and analysis are described in detail in [15]. Briefly, cells were seeded at a density of 0.07 cells per 100 μm^2 and left to adhere for 2 hours. Cells were then imaged every 4 minutes for 4 days. MDCK wild type cells (MDCK^{WT}) were winners in these competitions and their nuclei were labelled with H2B-GFP, while MDCK scribble knock down cells (MDCK scribble^{kd}) were the losers and labelled with H2B-RFP. Movies were then automatically analysed to track the position, state, and lineage of the cells using deep learning based image classification, and single-cell tracking, as detailed in [15]. Cell neighbours are determined using a Voronoi tessellation of the Delunay triangulation of nuclei.

Entropy of cell mixing. The entropy of mixing was calculated as the Shannon entropy of a two-state system, where the states considered are the cell types (winner/loser). The entropy was then calculated as $s = -P_1 Ln(P_1) - P_2 Ln(P_2)$ for each cell at each frame. Where

$P_1 = \frac{\text{no. winner neighbours}}{\text{total no. neighbours}}$ and $P_2 = \frac{\text{no. loser neighbours}}{\text{total no. neighbours}}$. The entropy of the whole system was then calculated as: $S =< s > / \sum cells$.

Cell fate analysis. Fate information for each cell is dynamically recorded to a file and analysed using a custom software written in Matlab to analyse experimental data [15].

REFERENCES

[1] Vincent, J.-P., Fletcher, A. G. & Baena-Lopez, L. A. Mechanisms and mechanics of cell competition in epithelia. *Nature Reviews Molecular cell biology* **14**, 581 (2013).

[2] Levayer, R. & Moreno, E. Mechanisms of cell competition: themes and variations. *J Cell Biol* **200**, 689–698 (2013).

[3] Morata, G. & Ripoll, P. Minutes: mutants of drosophila autonomously affecting cell division rate. *Developmental Biology* **42**, 211–221 (1975).

[4] Amoyel, M. & Bach, E. A. Cell competition: how to eliminate your neighbours. *Development* **141**, 988–1000 (2014).

[5] Chen, C.-L., Schroeder, M. C., Kango-Singh, M., Tao, C. & Halder, G. Tumor suppression by cell competition through regulation of the hippo pathway. *Proceedings of the National Academy of Sciences* **109**, 484–489 (2012).

[6] Madan, E. *et al.* Flower isoforms promote competitive growth in cancer. *Nature* 1 (2019).

[7] Moreno, E., Basler, K. & Morata, G. Cells compete for decapentaplegic survival factor to prevent apoptosis in drosophila wing development. *Nature* **416**, 755 (2002).

[8] Wagstaff, L. *et al.* Mechanical cell competition kills cells via induction of lethal p53 levels. *Nature Communications* **7**, 11373 (2016).

[9] Shraiman, B. I. Mechanical feedback as a possible regulator of tissue growth. *Proceedings of the National Academy of Sciences* **102**, 3318–3323 (2005).

[10] Levayer, R., Dupont, C. & Moreno, E. Tissue crowding induces caspase-dependent competition for space. *Current Biology* **26**, 670–677 (2016).

[11] Tyler, D. M., Li, W., Zhuo, N., Pellock, B. & Baker, N. E. Genes affecting cell competition in drosophila. *Genetics* **175**, 643–657.

[12] Yamamoto, M., Ohsawa, S., Kunimasa, K. & Igaki, T. The ligand sas and its receptor ptp10d drive tumour-suppressive cell competition. *Nature* **542**, 246 (2017).

[13] Levayer, R., Hauert, B. & Moreno, E. Cell mixing induced by myc is required for competitive tissue invasion and destruction. *Nature* **524**, 476 (2015).

[14] Díaz-Díaz, C. *et al.* Pluripotency surveillance by myc-driven competitive elimination of differentiating

cells. *Developmental Cell* **42**, 585–599 (2017).

[15] Bove, A. *et al.* Local cellular neighborhood controls proliferation in cell competition. *Molecular Biology of the Cell* **28**, 3215–3228 (2017).

[16] Gradeci, D., Bove, A., Charras, G., Lowe, A. R. & Banerjee, S. Single-cell approaches to cell competition: high-throughput imaging, machine learning and simulations. In *Seminars in Cancer Biology* (Elsevier, 2019).

[17] Nishikawa, S., Takamatsu, A., Ohsawa, S. & Igaki, T. Mathematical model for cell competition: Predator–prey interactions at the interface between two groups of cells in monolayer tissue. *Journal of Theoretical Biology* **404**, 40–50 (2016).

[18] Lee, S.-W. & Morishita, Y. Possible roles of mechanical cell elimination intrinsic to growing tissue from the perspective of tissue growth efficiency and homeostasis. *PLoS Computational Biology* **13**, e1005651 (2017).

[19] Tsuboi, A. *et al.* Competition for space is controlled by apoptosis-induced change of local epithelial topology. *Current Biology* **28**, 2115–2128 (2018).

[20] Abercrombie, M. Contact inhibition and malignancy. *Nature* **281**, 259 (1979).

[21] Graner, F. & Glazier, J. A. Simulation of biological cell sorting using a two-dimensional extended potts model. *Physical Review Letters* **69**, 2013 (1992).

[22] Fletcher, A. G., Osterfield, M., Baker, R. E. & Shvartsman, S. Y. Vertex models of epithelial morphogenesis. *Biophysical Journal* **106**, 2291–2304 (2014).

[23] Cadart, C. *et al.* Size control in mammalian cells involves modulation of both growth rate and cell cycle duration. *Nature Communications* **9**, 3275 (2018).

[24] Eisenhoffer, G. T. *et al.* Crowding induces live cell extrusion to maintain homeostatic cell numbers in epithelia. *Nature* **484**, 546 (2012).

[25] Kocgozlu, L. *et al.* Epithelial cell packing induces distinct modes of cell extrusions. *Current Biology* **26**, 2942–2950 (2016).

[26] Marinari, E. *et al.* Live-cell delamination counterbalances epithelial growth to limit tissue overcrowding. *Nature* **484**, 542545 (2012).

[27] S.A., G. *et al.* Mechanical stretch triggers rapid epithelial cell division through piezo1. *Nature* **543**, 118121 (2017).

[28] Kuipers, D. *et al.* Epithelial repair is a two-stage process driven first by dying cells and then by their neighbours. *J Cell Sci* **127**, 1229–1241 (2014).

[29] Rosenblatt, J., Raff, M. C. & Cramer, L. P. An epithelial cell destined for apoptosis signals its neighbors to extrude it by an actin-and myosin-dependent mechanism. *Current Biology* **11**, 1847–1857 (2001).

[30] Kucinski, I., Dinan, M., Kolahgar, G. & Piddini, E. Chronic activation of jnk jak/stat and oxidative stress signalling causes the loser cell status. *Nature Communications* **8**, 136 (2017).

[31] Basan, M., Risler, T., Joanny, J.-F., Sastre-Garau, X. & Prost, J. Homeostatic competition drives tumor growth and metastasis nucleation. *HFSP Journal* **3**, 265–272 (2009).

[32] Harris, A. R. & Charras, G. Experimental validation of atomic force microscopy-based cell elasticity measurements. *Nanotechnology* **22**, 345102 (2011).

[33] Harris, A. R. *et al.* Characterizing the mechanics of cultured cell monolayers. *Proceedings of the National Academy of Sciences* **109**, 16449–16454 (2012).

[34] Alt, S., Ganguly, P. & Salbreux, G. Vertex models: from cell mechanics to tissue morphogenesis. *Philosophical Transactions of the Royal Society B: Biological Sciences* **372**, 20150520 (2017).

[35] Latorre, E. *et al.* Active superelasticity in three-dimensional epithelia of controlled shape. *Nature* **563**, 203 (2018).

[36] Swat, M. H. *et al.* Multi-scale modeling of tissues using compucell3d. In *Methods in Cell Biology*, vol. 110, 325–366 (Elsevier, 2012).

[37] Li, J. F. & Lowengrub, J. The effects of cell compressibility, motility and contact inhibition on the growth of tumor cell clusters using the cellular potts model. *Journal of Theoretical Biology* **343**, 79–91 (2014).

[38] Lieberman, M. & Glaser, L. Density-dependent regulation of cell growth: an example of a cell-cell recognition phenomenon. *The Journal of Membrane Biology* **63**, 1–11 (1981).

[39] Azar, R., Susini, C., Bousquet, C. & Pyronnet, S. Control of contact-inhibition by 4e-bp1 upregulation. *Cell Cycle* **9**, 1241–1245 (2010).

[40] Hogan, C. *et al.* Characterization of the interface between normal and transformed epithelial cells. *Nature Cell Biology* **11**, 460 (2009).

[41] Kajita, M. *et al.* Interaction with surrounding normal epithelial cells influences signalling pathways and behaviour of src-transformed cells. *J Cell Sci* **123**, 171–180 (2010).

ACKNOWLEDGEMENTS

This work was supported two Engineering and Physical Sciences Research Council (EPSRC) PhD studentships to DG and AB. SB acknowledges support from the Royal Society (URF/R1/180187). AL and GC wish to acknowledge the support of BBSRC grant BB/S009329/1.